D5_8 Report on AVHRR aerosol demonstration dataset

Thomas Popp

DLR

8/25/2019

FIDUCEO has received funding from the European Union's Horizon 2020 Programme for Research and Innovation, under Grant Agreement no. 638822

1 Contents

2 Introduction

2.1 Scope

This document forms the deliverable D5.8 to report on the climate data record (CDR) over Europe and North Africa of aerosol optical depth (AOD) as retrieved from the AVHRR fundamental climate data record (FCDR) using a simple dark field Algorithm [**Error! Reference source not found.**]. The primary object of this data record is to assess and demonstrate how the sophisticated uncertainty information contained in the AVHRR easyFCDR dataset be propagated through a retrieval algorithm.

2.2 Version Control

Version	Reason	Reviewer	Date of Issue
0.1a	Draft structure iterated with EUMETSAT (similar report D5.9)	Frank Ruethrich	09.08.2019
1.0a	Issue of the document		25.08.2019

2.3 Applicable and Reference Documents

RD 1. FIDUCEO D2-4-d Uncertainty report for aerosol optical depth from AVHRR

RD 2. FIDUCEO D5.7 Metrological assessment of FIDUCEO CDRs

2.4 Glossary

Term	Description
AOD	Aerosol Optical Depth from the AVHRR 0.63 µm band
AERONET	Federated sun photometer network

3 The AVHRR Aerosol demonstration dataset

3.1 Dataset Definition and Spatiotemporal Coverage

AOD, namely aerosol optical depth is the vertical integral of aerosol extinction σ_e, calculated as AOD = $\int_0^{z_{max}} \sigma_e(z)\ dz$. From a polar orbiting satellite with sun-synchronous orbits such as those carrying the AVHRR instruments (NOAA, METOP platforms), one observation per day at nearly constant local time can be made (if cloud-free and within satellite swath of 2048 pixels). Thus the CDR consists of a time series of one snapshot per day for which the local time is nominally constant, but truly varies over the years and between different platforms due to orbit drift and different equator crossing times of different platforms. This needs to be kept in mind for applications by evaluating the systematic variations of the local time against typical AOD variation time scales. Overall, studies with ground-based continuous measurements have shown that differences between daily average and local morning overpass snapshot AOD are in many cases negligible. However, for specific cases (e.g. plumes, high AOD events) this may be critically different.

The processing chain consists of different levels. The major inversion of the input FIDUCEO easyFCDR Level1B product into Level2A AOD results is done on single pixels, but only for an automatically selected best-suited subset of them (cloud-free dark fields). From these aggregated superpixels (3x3 pixel cells) in sensor projection are averaged to provide the basic AOD product (Level 2B). Further aggregation to gridded cells (1 degree latitude, longitude, daily and monthly) is finally achieved with Level3 processing.

For a demonstration of uncertainty propagation from the easyFCDR L1B input a 10 year AOD record over Europe and North Africa was processed from two subsequent AVHRR/3 instruments onboard NOAA-16 and NOAA-18 as shown in table 1. The geographic coverage of the record consists only of pixels contained in the orbit L1B files over land within the rectangular area between latitudes of 30 and 75 degrees North and longitudes of 10 degrees West and 75 degrees East. Details of the methodology are described in RD-1.

Table 1: Temporal coverage and satellites that are included in this AVHRR Aerosol demonstration dataset

Satellite	Equator crossing time	Period processed
NOAA-16	14:30	01/01/2003 – 31/12/2005
NOAA-18	13:30	06/06/2005 – 31/12/2012

We show here for illustration first two example images of FIDUCEO AVHRR AOD monthly mean maps in January and August 2008 together with the number of days which contributed with valid observations (Figure 1) and for comparison with AOD maps obtained from the ensemble of 3 algorithms in Aerosol_cci for the AATSR instrument onboard ENVISAT. Obviously, the coverage to the North is limited in winter (due to low sun, large snow content and large cloud coverage, all factors which impede the application of the retrieval algorithm). One can also see that AOD values over Europe are typically somewhat larger in summer than in winder and lower in Scandinavia than in Central or Southern Europe. Also the coverage with valid days is not evenly distributed. The comparison with the AATSR maps shows overall similar value ranges (where both have coverage) and roughly similar patterns of higher AOD – note that ENVISAT has a morning orbit (equator crossing ~10:00) which leads to lower sun and coverage in winter some shifts of patterns moved between

the local overpass times. Also differences come from differences in the sampling of AATSR with its 512 km swath width (repeat cycle ~ 6days) is 4 times weaker than AVHRR with 2048 km swath (repeat cycle every 1-2 days).

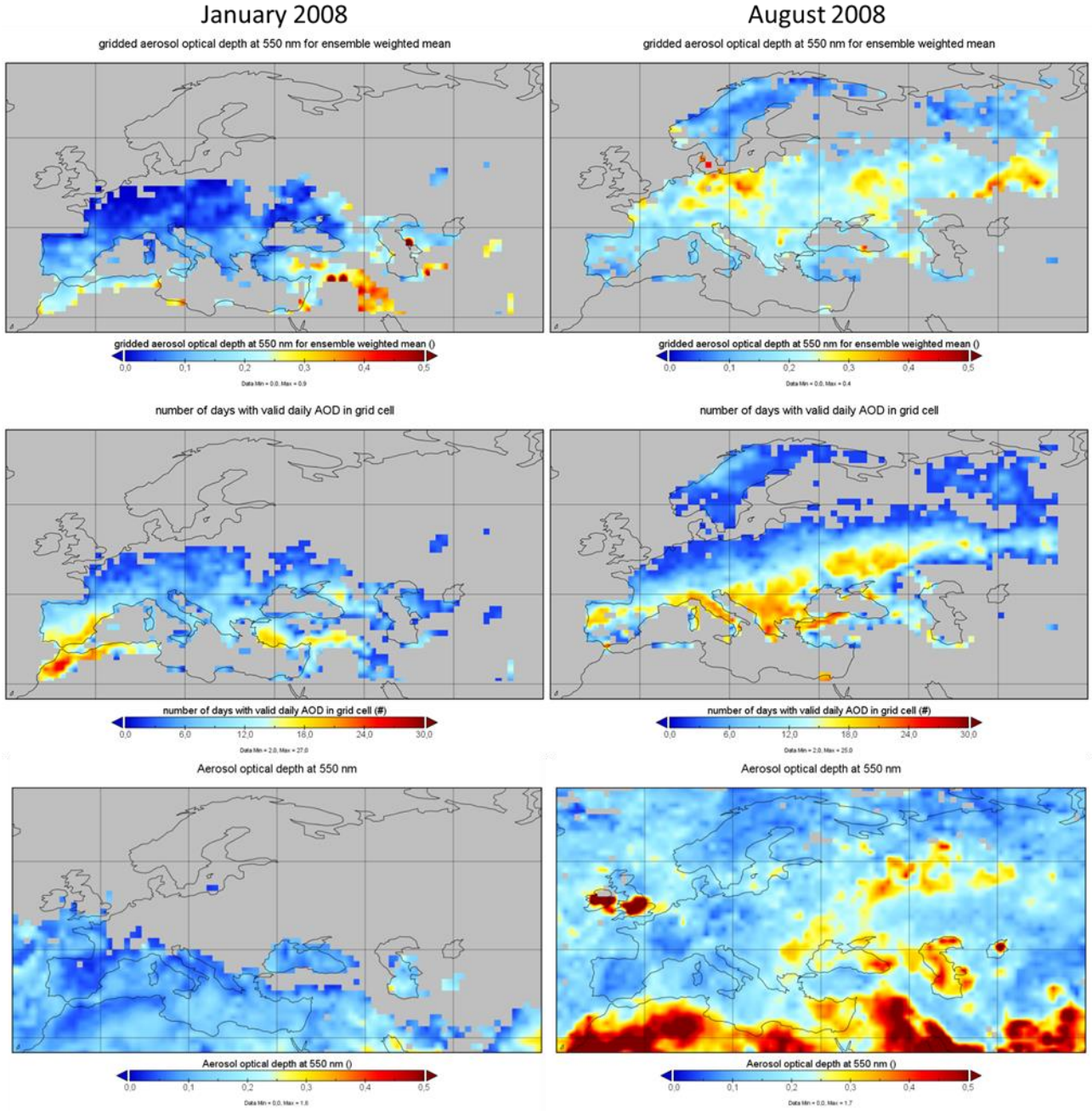

Figure 1: *AVHRR AOD550 monthly mean maps (upper line) for January and August 2008 with numbers of days contributing (lower line) and comparison AOD550 maps of the AATSR ensemble*

The sequence of processing levels is illustrated in Figure 2 starting from a single orbit (at 11:04:36) where the single pixel L2A product over suitable selected cloud-free dark field pixels is processed – this intermediate product is not handed out to users, since better quality is achieved by averaging 3x3 pixels into superpixels (L2B product, requesting a minimum of 3 valid pixels within). 14 orbits are then averaged over one day into the 1 degree L3 daily product (requesting a minimum of 5 pixels within a grid cell) and further all days are averaged into an L3 monthly product (requesting a minimum of 2 days with valid observations).

The day chosen for a case study (see more detail in section 4.2) was selected to include a typical large scale cloud system (to demonstrate cloud masking) and large cloud-free areas where for a few days transport of fire emissions from Russia into Central Europe was observed, which is visible in a band North-West of the Black sea during that day (but no longer in the monthly average).

The FIDUCEO AVHRR AOD CDR is provided as netCDF format with a minimal set of CF-compliant metadata so that a user can rely on the FIDUCEO reader software.

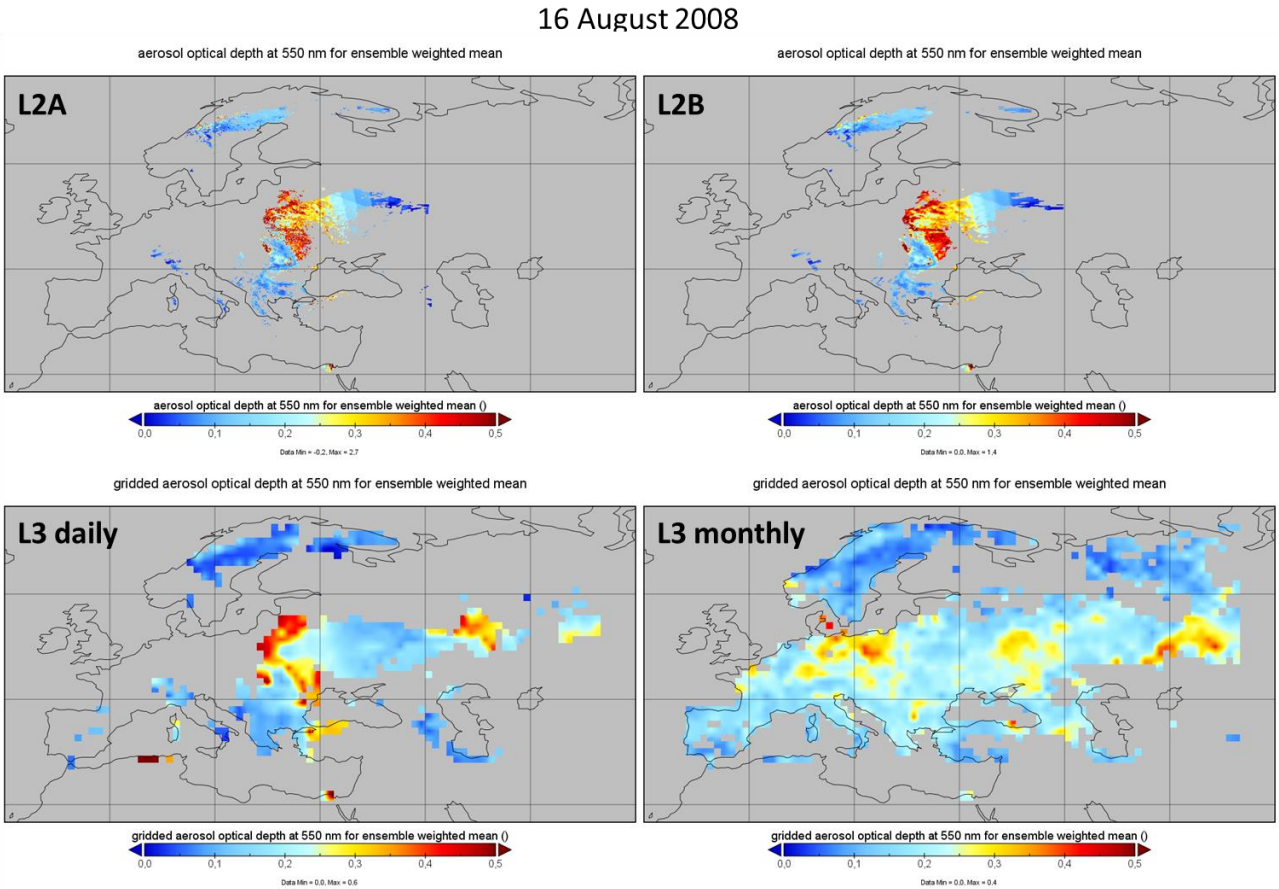

Figure 2: *propagation of AVHRR AOD through the processing levels from top left to bottom right (L2A, L2B, L3 daily, L3 monthly)*

The variables contained in the FIDUCEO AVHRR AOD product files are explained in table 1.

Table 2: Temporal coverage and satellites that are included in this AVHRR Aerosol demonstration dataset

variable	explanation	L2A	L2B	L3D	L3M
latitude	Geographic latitude	X	x	x	x
longitude	Geographic longitude	X	x	x	x
lat_bnds	Grid cell boundaries			x	x
lon_bnds	Grid cell boundaries			x	x
time	Time in seconds since 1.1.1970 00:00:00	X	x		
Satellite zenith angle	Satellite zenith angle in degrees	X			
Solar zenith angle	Solar zenith angle in degrees	X			
Relative azimuth angle	Relative azimuth angle in degrees	X			
Scattering angle	Scattering angle in degrees	X			
NUMBER	Pixel / orbit number in superpixel or grid cell		x	x	x
NUMBER0	Available pixel number			x	x
NUMBER1	Valid pixel number			x	x
NUMBERDAYS	Number of day with valid daily AOD				x

Main AOD output variables					
AODENSB	Weighted mean ensemble AOD	X	x	x	x
AOD	36 member AOD ensemble	X	x	x	x
AODCLIM	AOD of selected climatology mix	X	x	x	x
AODBEST	Filtered AOD with AOD_UNCERTAINTY < 0.2			x	x
AODBEST2	Filtered AOD with AOD_UNCERTAINTY < 0.1 OR 20% of AODENSB			x	x
Main AOD uncertainty variables					
AOD_UNCERTAINTY	Total AOD uncertainty	X	x	x	x
AOD_UNCERTAINTY1	AOD uncertainty due to reflectance effect (no. 1)	X			
AOD_UNCERTAINTY1_common	common uncertainty due to reflectance effect	X			
AOD_UNCERTAINTY1_indep	independent uncertainty due to reflectance effect	X			
AOD_UNCERTAINTY1_struct	structured uncertainty due to reflectance effect	X			
AOD_UNCERTAINTY2	AOD uncertainty due to albedo effect (no. 2)	X			
AOD_UNCERTAINTY2_common	common uncertainty due to albedo effect	X			
AOD_UNCERTAINTY2_indep	independent uncertainty due to albedo effect	X			
AOD_UNCERTAINTY2_struct	structured uncertainty due to albedo effect	X			
AOD_UNCERTAINTY3B	AOD uncertainty due to ensemble spread (weightsum normalized)	X			
AOD_UNCERTAINTY4	AOD uncertainty due to cloud masking uncertainty	X			
AOD_UNCERTAINTY_common	Uncertainty due to all common effects	X	x	x	x
AOD_UNCERTAINTY_common_12	Uncertainty due to common effects (1, 2) with full temporal correlation			x	x
AOD_UNCERTAINTY_common_3b	Uncertainty due to common effect (3) with weekly correlation			x	x
AOD_UNCERTAINTY_indep	Uncertainty due to all independent effects	X	x	x	x
AOD_UNCERTAINTY_struct	Uncertainty due to all structured effects	X	x	x	x
AOD_UNCERTAINTY_random	Hypothetic uncertainty assuming all pixels fully independent		x	x	x
AOD_UNCERTAINTY_correlated	Hypothetic uncertainty assuming all pixels fully correlated		x	x	x
AOD_UNCERTAINTY_sampling	Estimated uncertainty due to spatial sampling gaps			x	x
AOD_UNCERTAINTY_sampling_days	Estimated uncertainty due to temporal sampling gaps				x
Further AOD variables					
AODENS	Mean ensemble AOD	X	x		
AOD1	AOD with strict cloud probability threshold (15%)	X	x		
AOD2	AOD with weak cloud probability threshold (50%)	X	x		
AOD_UNCERTAINTY3	AOD uncertainty due to ensemble spread (not normalized)	X			
Climatology_mix	Aerosol mix most likely in multi-model ensemble	X			
Diagnostic variables					
PCLD	Cloud probability (%)	X			
Albedo, Albedo2	Surface directional albedo	X	x	x	x
Alb_u_i, Alb_u_c, Alb_u_s	Uncertainty components of albedo	X			
NDVI, NDII	Vegetation indeces	X			
B-factor values (optional testing)	Conversion factor mid-IR to red band	X			
Dark field used	Mask of selected dark fields	X			
R1, R2, R3.7	Input reflectances	X			
Ref3_u_common, _indep, _struct	3.7 µm band uncertainty contributions	X			
Further numbers	For internal control		x	x	x

3.2 Retrieval Method

The algorithm used to produce the AVHRR Aerosol demonstration dataset is described in D2.4-d.

The AVHRR instrument, which was designed for cloud and land observations, is a weak instrument if it is used for the retrieval of a Climate Data Record (CDR) of Aerosol Optical Depth (AOD) over land, because of its small information content with practically only one useful channel with uncertain calibration. However, AVHRR offers a long historic record back to 1978 from the series of instruments flown on NOAA and METOP platforms.

AOD can be inverted from top-of-atmosphere (TOA) reflectance measurements in the red band, (directional) surface albedo estimated from the mid-infrared channel at 3.7 µm and a vegetation index, and by assuming optical properties of atmospheric aerosol (aerosol type) from a multi-model based climatology.

3.3 Challenges

For the retrieval of AOD over land from AVHRR single channel measurements the weak radiometric calibration poses a first difficulty, which can lead to slightly negative AOD values in the lowest processing level L2A (which are allowed to avoid breaking the distribution of AOD values artificially at the wrongly calibrated zero value). The second major challenge lies in the estimation of directional surface albedo, so that in the inversion the signal contribution from aerosols and from the surface can be separated. This is still the largest challenge for this simple method (and needs more work beyond the FIDUCEO demonstration case study). The third challenge lies in propagating uncertainties through the processing levels while being able to take into account their different correlation structures – here the FIDUCEO easyFCDR L1B dataset provides all necessary information to do this propagation rigorously.

3.4 Dataset Validation

3.4.1 Validation Data

For the validation of the FIDUCEO AVHRR AOD dataset we use the common standard in the aerosol retrieval community, which is comparison to ground-based sun photometer measurements. These can directly measure exactly the same quantity, namely Aerosol Optical Depth (AOD), with very high accuracy (~0.01) by directly looking at the sun. A continuous network is coordinated by NASA (AERONET, Holben, et al., 2008), form which the latest processed version v3 of quality controlled sun photometer measurements at ~200 permanent stations back to mid-1990s can be obtained. This provides a unique reference dataset. However, even this unique reference has its limitations in global coverage (less so in Europe and the US) and for larger pixels or grid cells there is a representativity issue of a point station measurement against a large area covered from satellite – this becomes a significant limitation for 1 degree lat-lon grid cells (imagine how different environmental conditions can be within a rectangular area of ~110 km size).

3.4.2 Method

We statistically analyse here first a set of density scatter plots to determine the quality of the dataset including diagnostic plots of the AOD difference between AVHRR and AERONET as function of some retrieval parameters (geometry, vegetation index), scatter plots of AOD AVHRR vs. the AERONET reference (within the commonly used matching window of ±30 min and ±50km), and density scatter plots for all years and for the different levels of the processing chain (L2A, L2B, L3_daily) – the latter is shown here in figure 3.

Then, we assess the uncertainties by comparing probability functions of the difference between AVHRR and AERONET AOD (a very good estimate of the true error) with the distributions for the propagated uncertainties through the processing chains levels (L2A, L2B, L3_daily, repeated as figure 4 in this report) and for all years, and for illustration also show compared with two hypothetic distributions which were achieved by propagating all uncertainties assuming either their full correlation between pixels (all common) or full independence (all random) – shown in figure 5 of this report. We calculate then the quantity $\Delta = \frac{AOD_{AVHRR} - AOD_{AERONET}}{u(AOD)}$ (for a Gaussian distribution Δ values of 68.3% of all pixels should fall within the interwall [-1, +1]) and provide those fraction values in two tables for all years and for 2008 for all processing chain levels. In the denominator we neglect here the very small Aeronet AOD uncertainty and also the difficult to estimate representativity error between the station and pixel area observations.

3.4.3 Results

The full validation of the AVHRR Aerosol demonstration dataset (retrieved AOD and its uncertainties) is described in D5.7. We show here the excerpt for one year (2008).

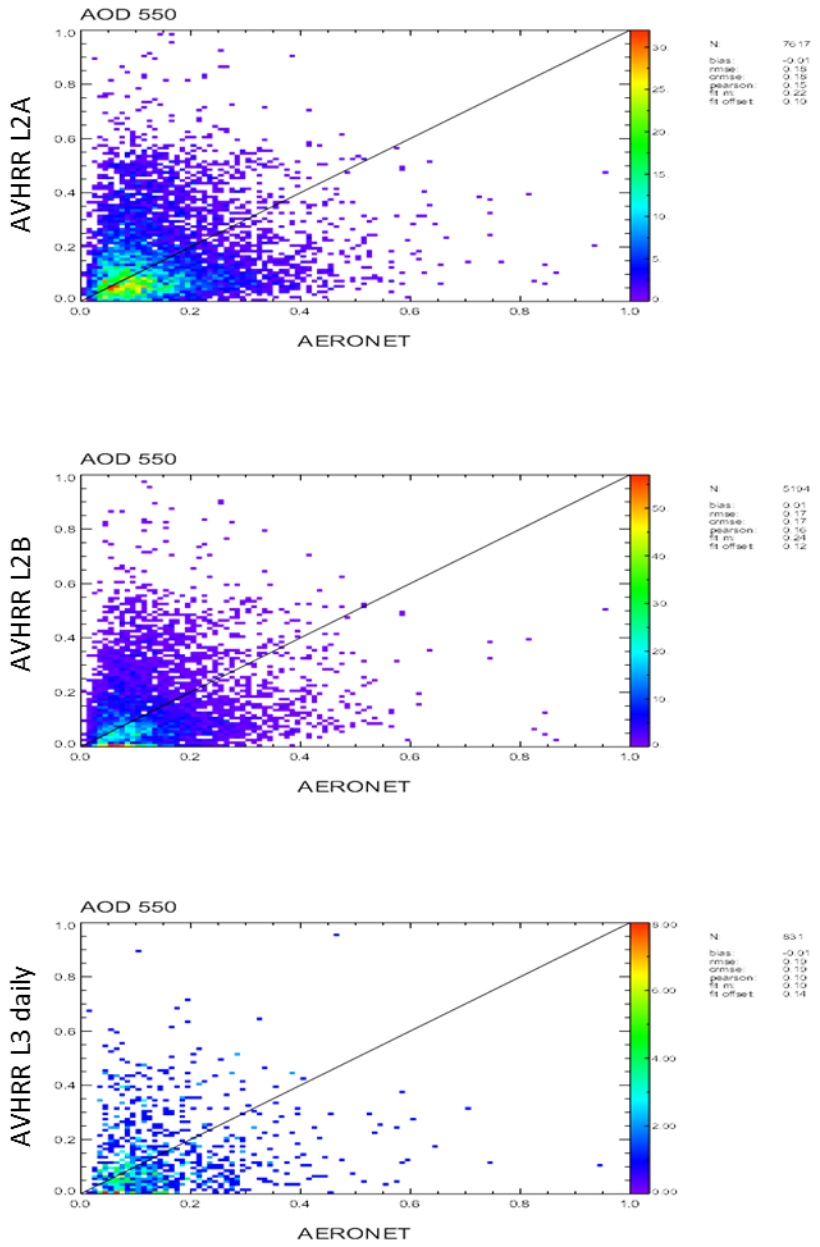

Figure 3: AOD *density scatter plots of AVHRR vs. AERONET for 2008 and different processing levels*

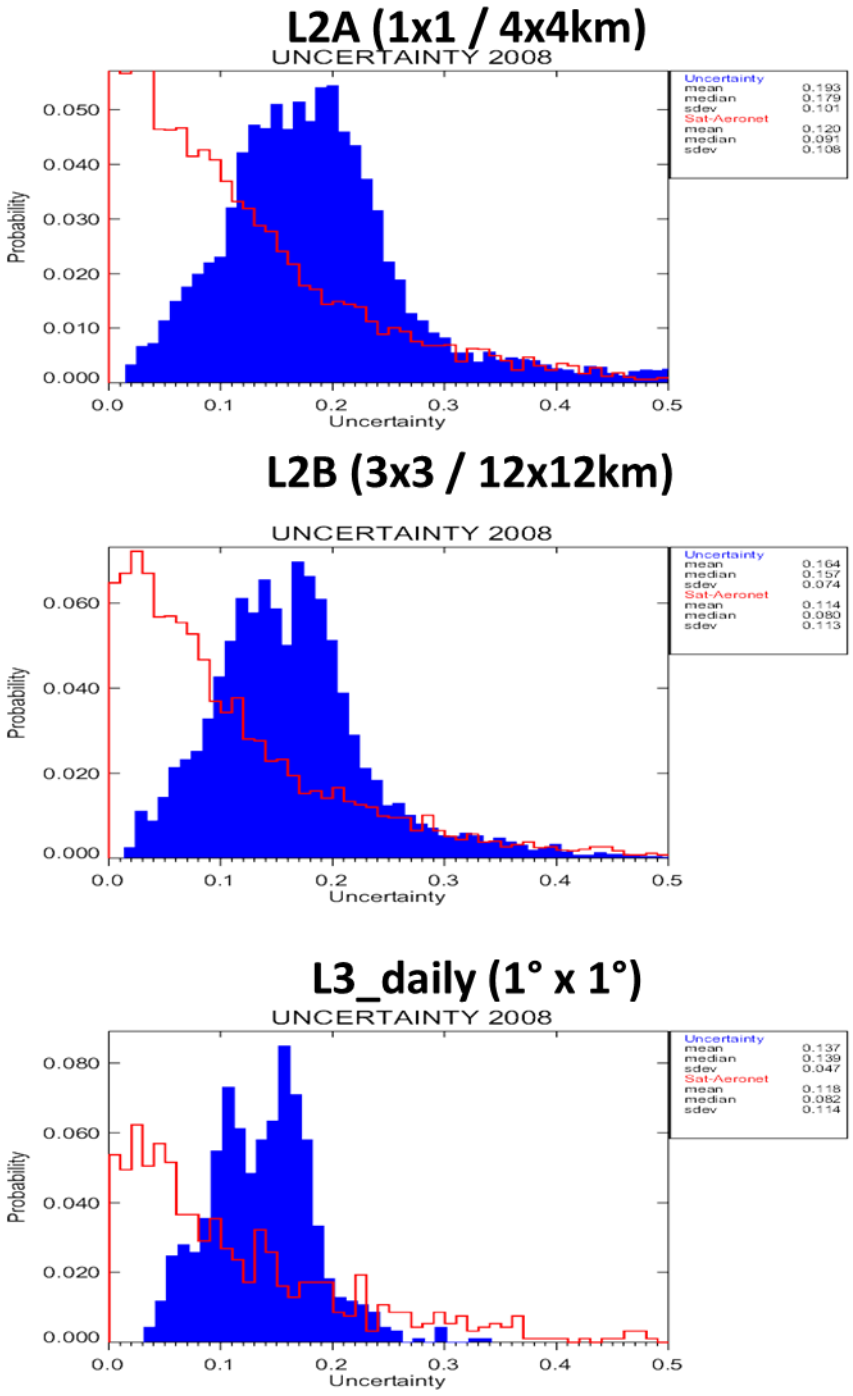

Figure 4: probability distributions of estimated true error and propagated uncertainties for 2008 (all levels)

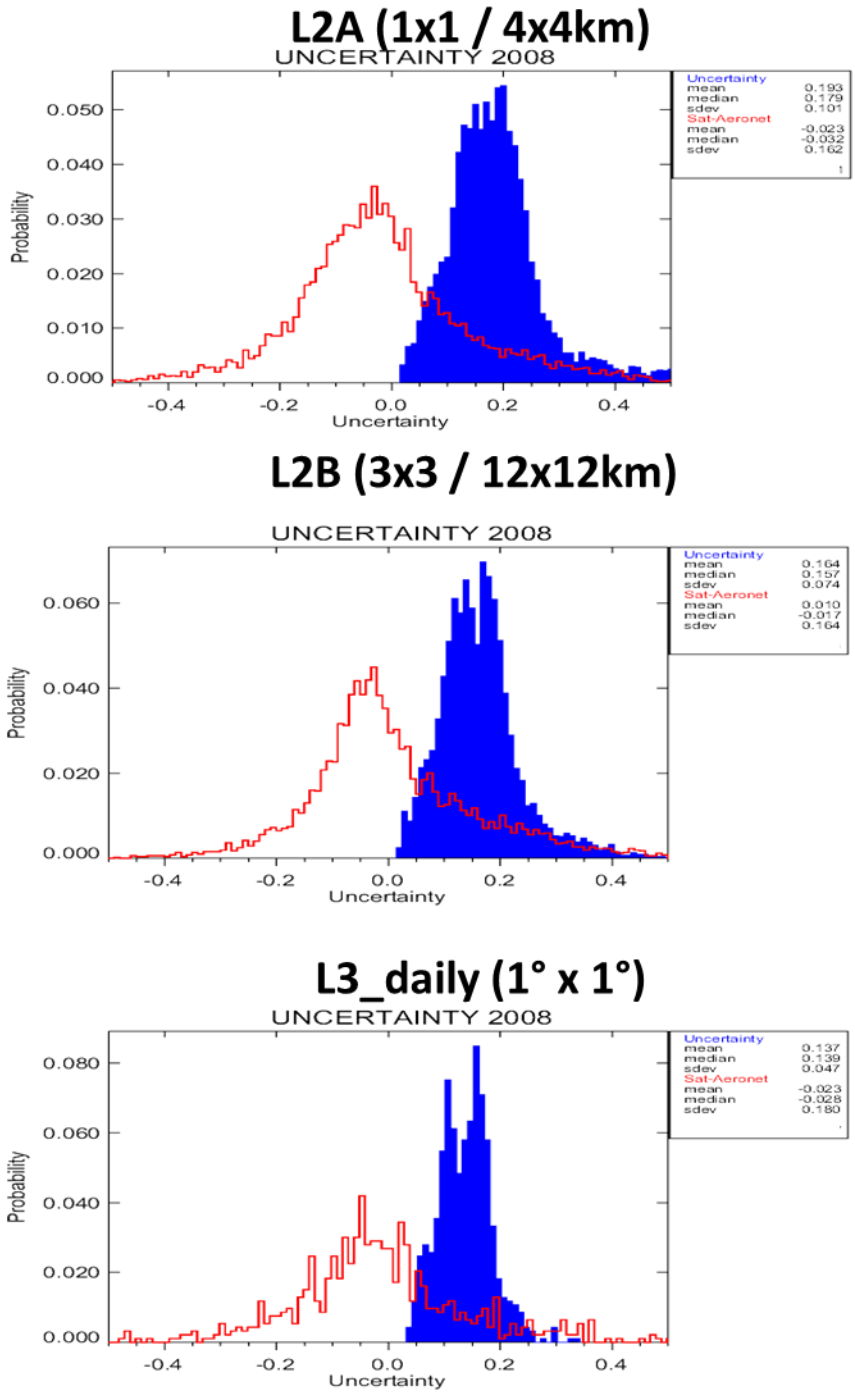

Figure 5: probability distributions of absolute estimated true error and propagated uncertainties for 2008 (all levels)

For the superpixels (L2B product) the fraction of pixels where the Δ value falls within [1-, +1] lies in most years slightly above 70% which would indicate an under-estimation of uncertainties compared to true error estimates under the assumption of a Gaussian distribution of the errors. For the different processing levels the fractions decrease from above 70% to 56% which would indicate an over-estimation of uncertainties. As can be seen in the probability functions (figure 5) the error distributions are not completely Gaussian so that the theoretical best assumption of 68.3% is likely to be shifted and then overall a slight over-estimation of

uncertainties is concluded with decreasing tendency over the processing levels (as also seen in the mean values of absolute errors versus uncertainties in figure 4).

4 Spatiotemporal Variability of AOD

4.1 Time series

We show here the monthly mean time series aggregated for the whole of Europe (over land only, 10W – 50E, 35 – 60 N, excluding parts of Algeria and Morocco in this rectangle). We compare with a multi-sensor merged datasets including the period 2003 – 2012 (Sogacheva, et al., 2019, AMTD, in review). Figure 6 shows the good agreement of the range of values (with smaller minima, possibly due to different coverage), and also good agreement in the seasonal cycle; even a double peak in summers is visible, while intra-annual maxima / minima variation disagrees (likely due to the different sampling).

We can also see that the overlap of the AVHRR record parts from the two platforms NOAA-16 (black) and NOAA-18 (red) in 2005 (7 months) in figure 6 is very good.

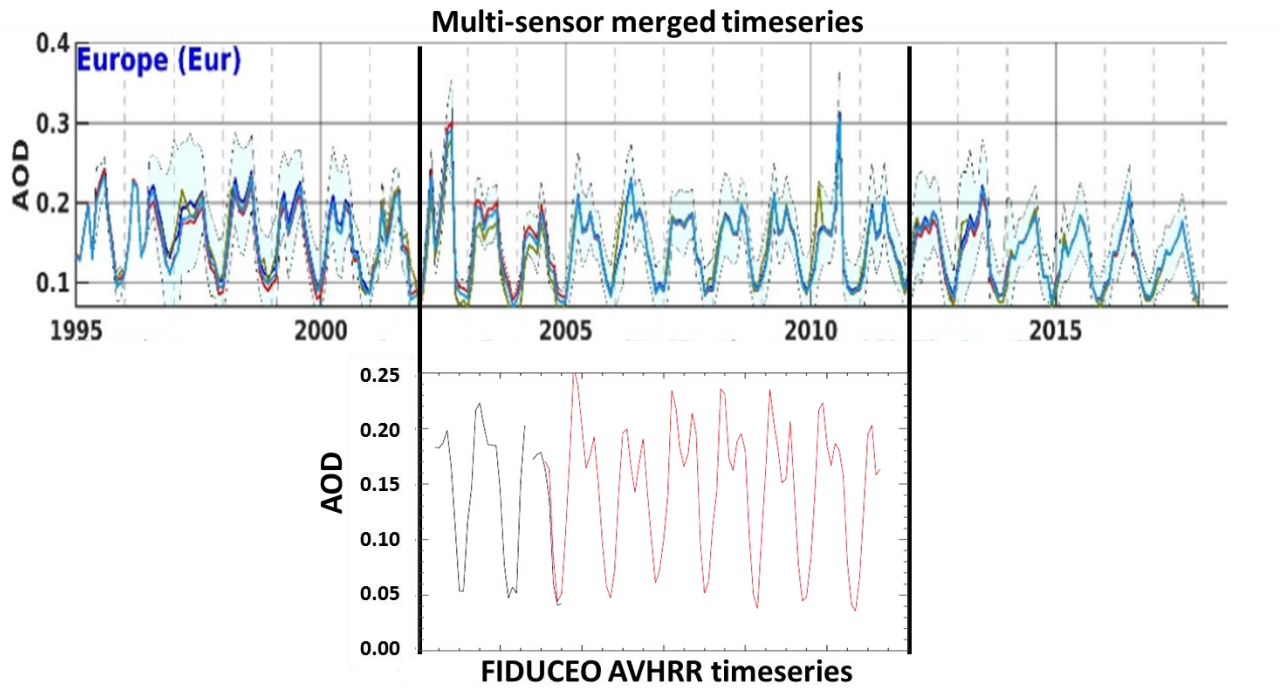

Figure 6: monthly AOD *time series over Europe (land only) from FIDUCEO AVHRR AOD (bottom) and multi-sensor merged dataset AOD (Sogacheva, et al., 2019)*

We also look at the all-Europe annual records from the 15 individual datasets used for the merged dataset and the FIDUCEO AVHRR record in figure 7. The average value agrees quite well. The slow decrease visible in all of the merging datasets can also be seen in the record of full years from NOAA-18 (2006 – 2012, with 7 data points only any trend analysis needs to be treated with caution!). It vanishes in the combined AVHRR dataset from NOAA-16 and NOAA-18 (with 11 points only, where some of them even lack part of the year). Also note the spread between the 15 datasets used for the merged dataset and that among them AVHRR pieces of another AVHRR record (by Andy Sayer / NASA) are shown in green in fig. 7.

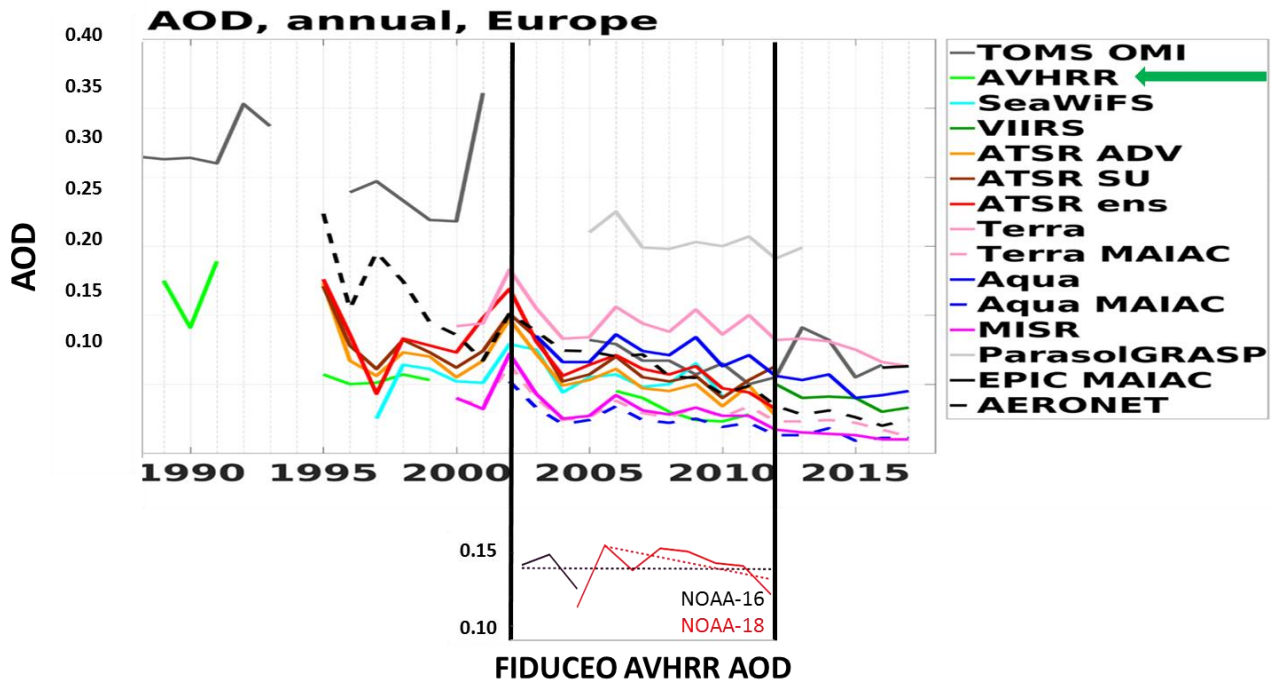

Figure 7: time series of annual mean AOD over Europe from the 15 different satellite records used for the merged dataset (upper part, from Sogacheva et al., 2019) and from FIDUCEO AVHRR AOD (lower part); the ground-based AERONET record is also included in dashed line in the upper part, while dashed lines in the lower part indicate the "trends".

4.2 Case study

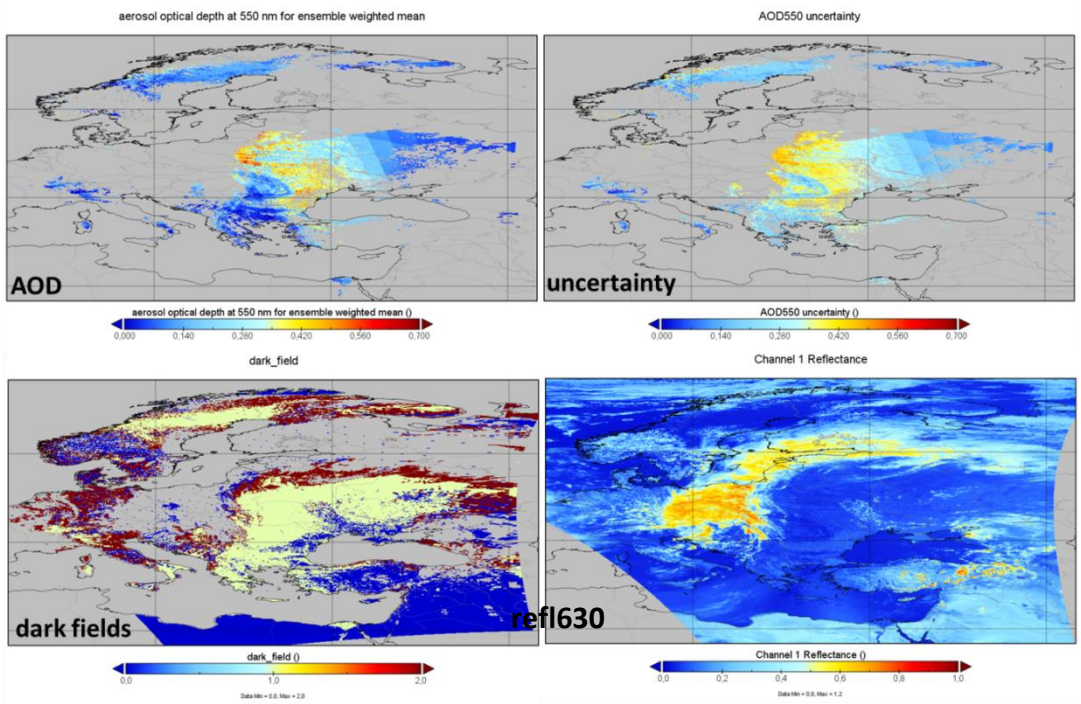

Figure 8: *Example scene (NOAA-18, 16.08.2008): upper left: retrieved AOD; upper right: total AOD uncertainty; lower left: selected dark fields (yellow: from strict cloud masking, red: from weak cloud masking, blue: cloud-free but not used); lower right: top of atmosphere reflectance in the AVHRR red band.*

To illustrate the uncertainty calculation, step-by-step results for one orbit (NOAA-18, 16.08.2008 over Central Europe) are shown here. During this day heavy fire activity happened in Eastern Europe (as proven by AATSR satellite images, not shown here), from which aerosols were transported to Central Europe. Figure 8 shows an obvious cloud system (orange / yellow) and areas with broken clouds (e.g. over Germany and Western Scandinavia) in the visible image (red band). Inverted AOD and its total uncertainty are also shown together with the selected dark pixels used for the inversion.

The four dominant uncertainty contributions are shown in Figure 9 due to the reflectance inversion, due to the estimated surface albedo, due to the weak knowledge of the aerosol mixture, due to cloud masking uncertainties (note the different scales).

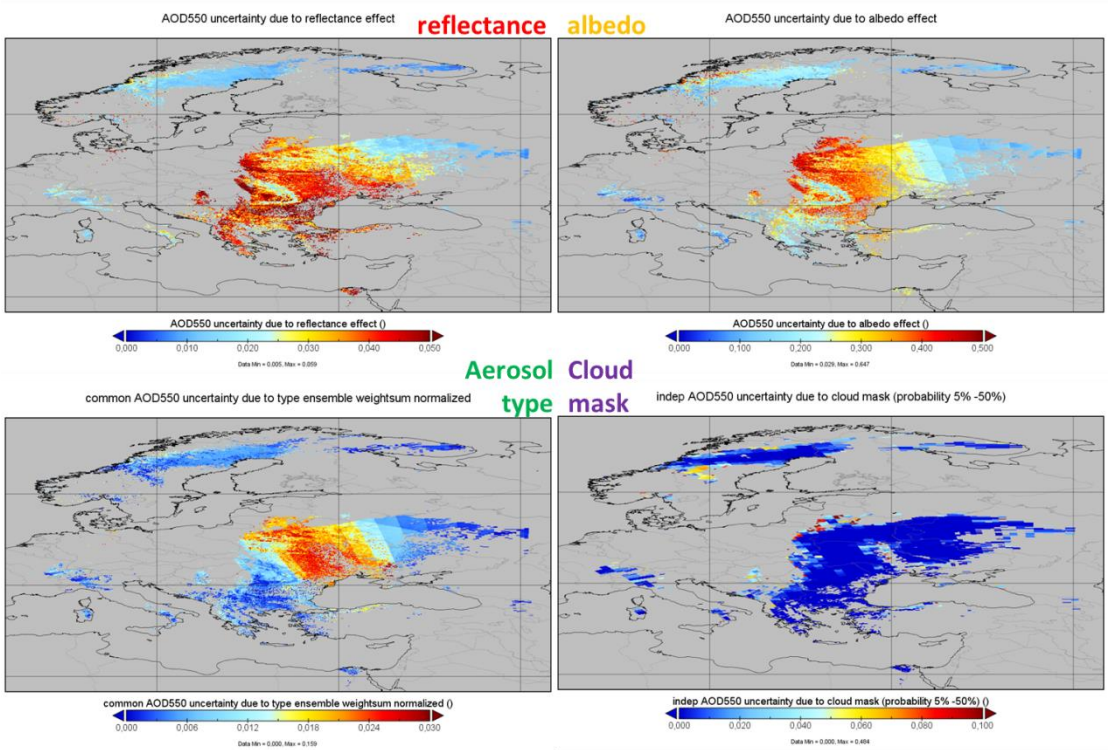

Figure 9: *Example scene (NOAA-18, 16.08.2008): Dominant uncertainty contributions, from upper left to lower right: reflectance term, albedo term, aerosol type term, cloud mask term.*

Calculating the cloud mask induced uncertainty is shown in the Figure 10. The difference of retrieved AIOD maps based on two different cloud masks (with two different cloud probability thresholds) is exploited to estimate the cloud-mask induced uncertainty. The two probability threshold values have been determined experimentally by testing several values, so that sufficient coverage can be achieved while the main effects due to broken clouds and cloud edges can be seen. Note that the resulting AOD and all other uncertainties are calculated on the basis of the more conservative (i.e. safer) cloud probability threshold.

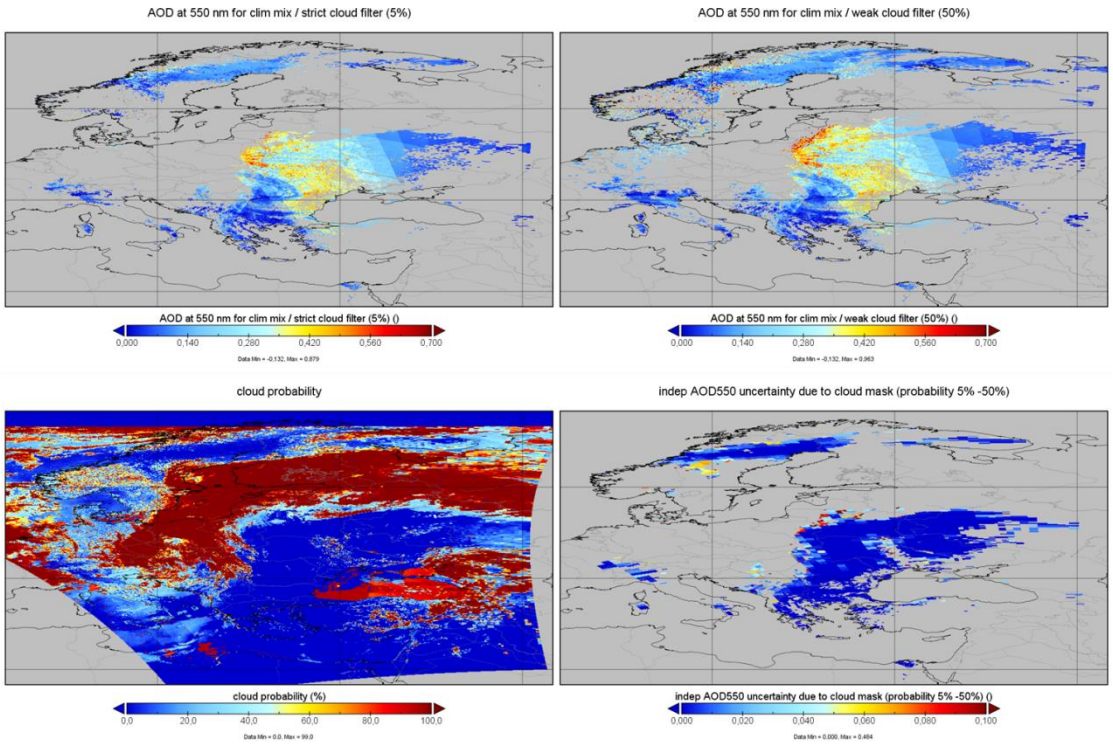

Figure 10: *Example scene (NOAA-18, 16.08.2008): cloud mask induced AOD uncertainties, from upper left to lower right: average AOD with strict cloud filtering; average AOD with weak cloud filtering, cloud probability retrieved, difference of the AOD maps.*

In Figure 11, the propagation of AOD uncertainties with different correlation structures is illustrated. While common uncertainties undergo no reduction at all, the independent (random) uncertainties are subject to a major noise reduction.

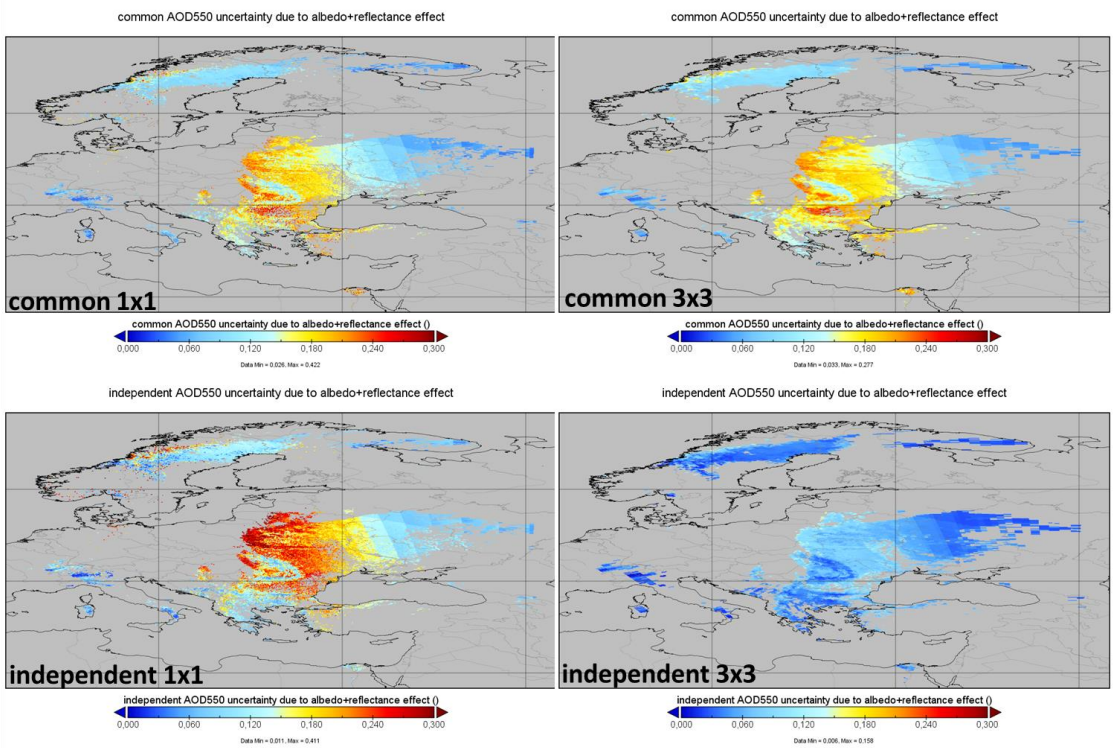

Figure 11: *Example scene (NOAA-18, 16.08.2008): Propagating uncertainty components from pixels (1x1, left) to super-pixels (3x3, right) for different correlation structures: common component (upper line), independent component (lower line).*

The propagation of total AOD uncertainties to super-pixels (3x3) and to gridded values (1 degree, with only one orbit as input) is shown in Figure 12. Clearly, uncertainties get reduced by the averaging, but not everywhere the reduction is the same. Finally, the resulting total AOD uncertainty is compared to imaginative total uncertainties, which would come out if all uncertainties were considered fully independent ("assuming all random") or fully correlated ("assuming all correlated"). Obviously, the uncertainties propagated with the wealth of the FIDUCEO L1B uncertainty correlation structures fall between the two extremes while the effect of noise reduction differs in different conditions (AOD, surface brightness, geometry, cloudiness).

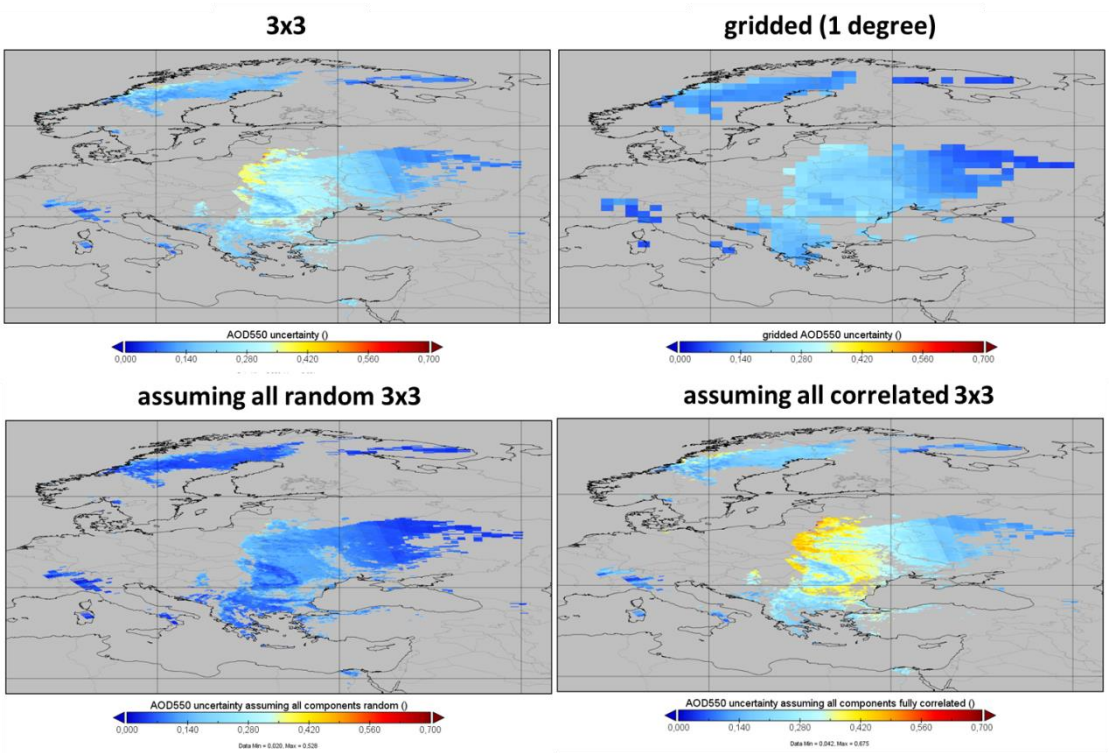

Figure 12: *Example scene (NOAA-18, 16.08.2008): AOD uncertainty on super-pixel (3x3) resolution (upper left) and daily gridded (upper right, with one orbit input only). Fictional 3x3 uncertainties are shown in the lower line right), are fictionally assuming no / random (left) or full correlation (right).*

5 Applicability

5.1 Using CDR uncertainties

The use of the CDR uncertainties can be directly derived from the intrinsic use of the uncertainties during the propagation of the different processing levels where in each application a user needs to take similar steps. On all levels of the AVHRR AOD product the user receives total uncertainties (which can be used directly for example in a data assimilation scheme or to ascertain a confident range around values). But also the contributions following up from the input L1B component are provided which allow a user to take their different correlation structures into account when averaging spatially or temporally. The independent contribution is fully random and can be added up by calculating the square root of the sum of squared pixel uncertainties divided over the number of pixels (this leads to noise reduction increasing with the number of averaged pixels or grid cells – first equation below). The common contribution is always assumed to be globally correlated, so that uncertainties from different pixels can be simply averaged (no noise reduction can thus be achieved – second equation below). In between the structured contributions are fully correlated along one line (again calculate the average uncertainty per line) while they are correlated with decreasing strength between lines (correlation coefficients dropping from 1 to 0 over 40 L2A lines or 13 L2B lines). Here the squared sum of two lines needs to be extended with an additional term of twice the product of the two averaged line uncertainties times the correlation coefficient as function of the distance between the two lines (3rd equation below). For the gridded datasets all structured contributions lose their correlations and are treated as independent, with one exception: The aerosol type ensemble uncertainty (number as effect 3) is fully correlated within a 1 degree grid cell and within a week (i.e. calculate simple uncertainty averages and only for larger areas than 1 degree or larger periods than 1 week treat them as independent .

$$\underset{\text{random}}{\text{independent}} \quad u(AOD_{3x3}^{unstructured}) = \frac{1}{N_{dark\,fields}} \cdot \sqrt{\sum_{dark\,fields} u(AOD_{dark\,field\,i})^2}$$

$$\underset{\text{global}}{\text{common}} \quad u(AOD_{3x3}^{structured}) = \frac{1}{N_{dark\,fields}} \cdot \sqrt{\sum_{dark\,fields} u(AOD_{dark\,field\,i})^2 + 2\sum_{i>j}\sum C_{ij}\, u(AOD_{dark\,field\,i})\, u(AOD_{dark\,field\,j})}$$

$$\underset{\text{scaled}}{\text{structured}} \quad u(AOD_{3x3}^{strutured}) = \frac{1}{N_{dark\,fields}} \sum_{dark\,fields} u(AOD_{dark\,field\,i})$$

5.2 Possible use of the aerosol type ensemble

We have also analysed the feasibility of using uncertainty to select best pixels (as was requested at AEROSAT / AEROCOM meetings by model users). The key issue is whether a filtering with low uncertainty entails the risk of supressing high AOD values. As part of the product files we provide for the gridded processing levels (L3 daily, monthly) a variable AODBEST filtered with AOD uncertainty < 0.15. As shown in figure 13 for our case study example day of 20080816 this filtering keeps the key AOD feature (which agrees also with the

daily MODIS map shown in the lower right, but with typically significantly larger AOD values in the plume transported from East Europe), but somewhat reduces the coverage (not too critically). Uncertainties above 0.15 are indicated in yellow in the upper right plot.

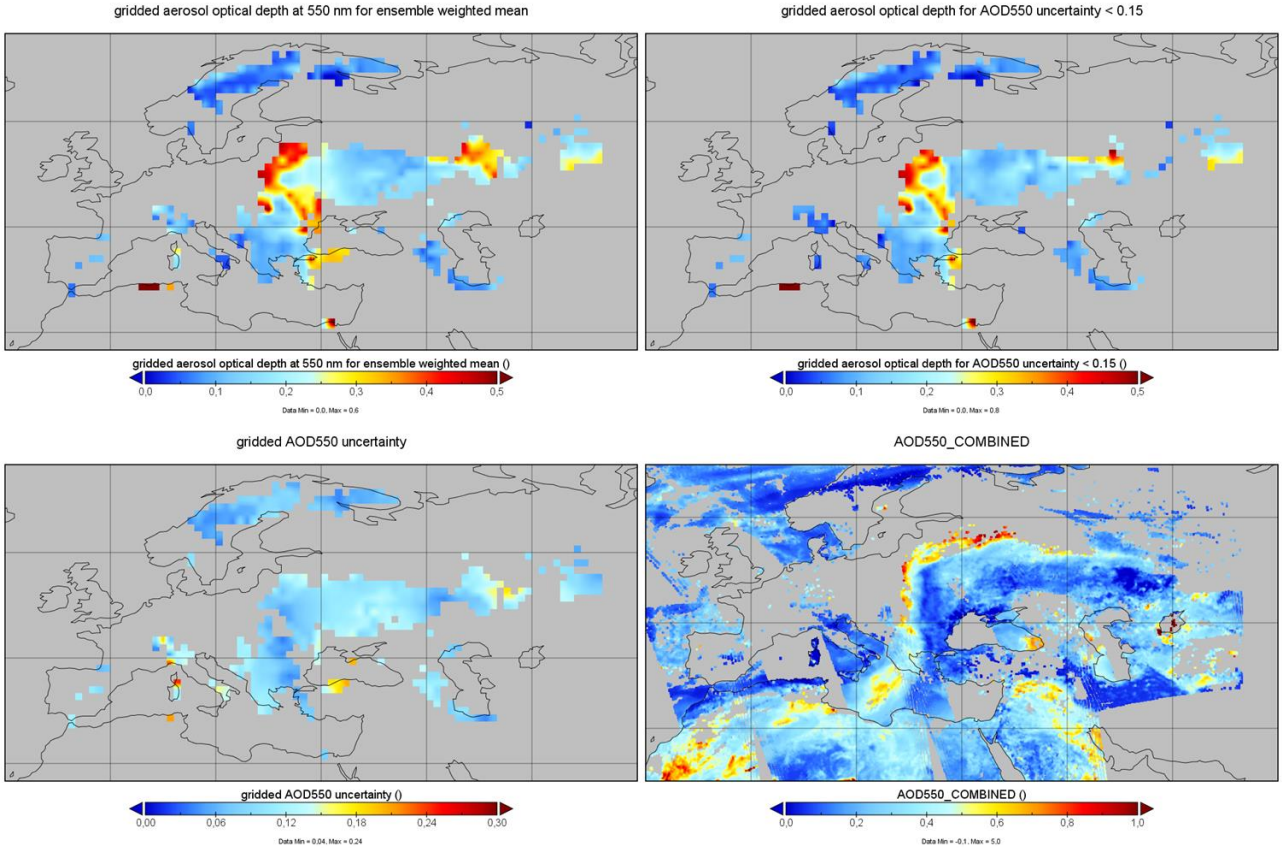

Figure 13: example of AODBEST (filtered with AOD uncertainty < 0.15) in upper right versus the unfiltered daily AOD (upper left), with calculated underlying uncertainties (lower left) and for comparison a MODIS AQUA afternoon map of the same day (lower right).

We also assess in figure 14 the density scatter for the uncertainty-filtered AOD. This analysis for 2008 shows that despite of growing uncertainty with increasing AOD, the retrieval error shows no statistical dependence to the propagated uncertainty, while the filtered product keeps about the same statistical validation properties. In conclusion, we state that a user needs to be careful and analyse for the specific application the impact of filtering with AOD uncertainty.

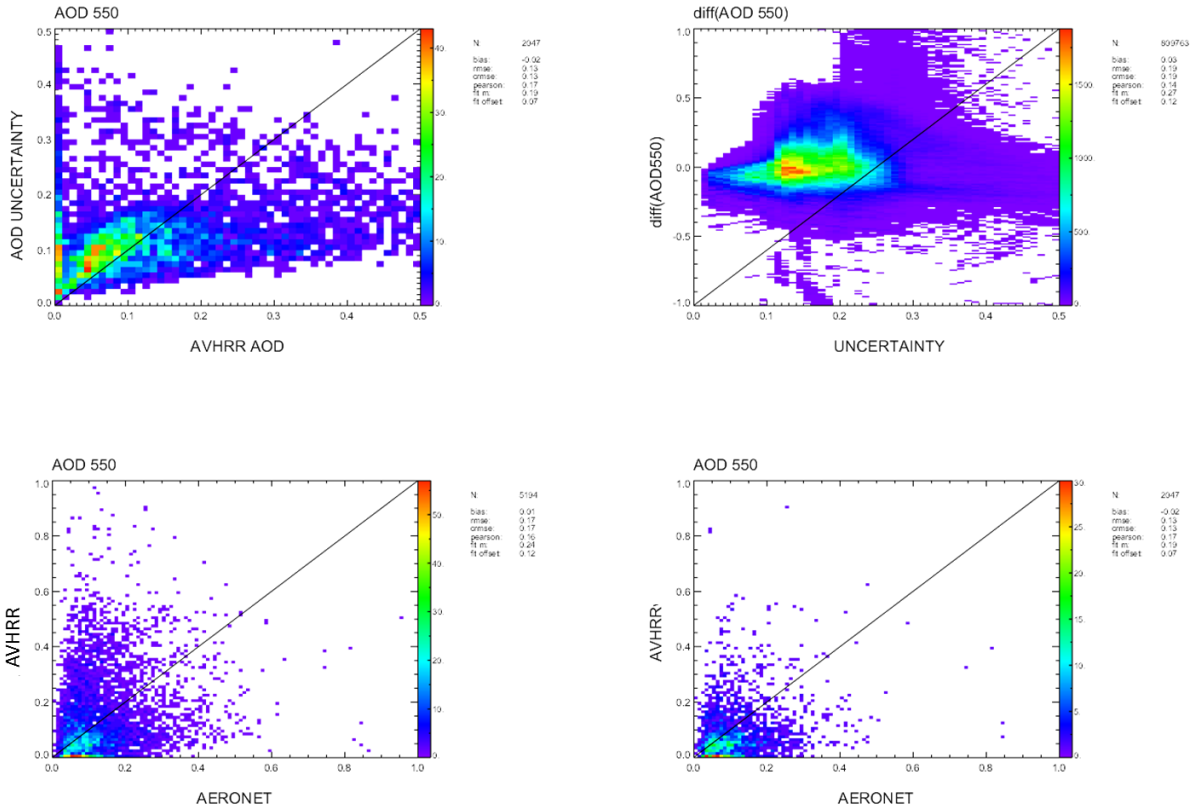

Figure 14: assessment of impact of filtering with AOD uncertainty by various density scatter plots: dependence of uncertainty to retrieved AOD (upper left), dependence of retrieval error to uncertainty, validation plots of full product (lower left) and of filtered product (lower right).

Finally, we want to point to another property of the product, which is the ensemble of AOD solutions for 36 different aerosol types (mixtures of 4 basic components which are meant to span the realistic range of optical aerosol properties). A user can also propagate all 36 solutions through an application and afterwards calculate the spread of solutions for this ensemble (either evenly distributed which means no knowledge on the aerosol type is assumed) or by using the climatology mix / AOD for the most likely aerosol mix which are also provided in the product files. As done for calculating the uncertainty due to the uncertain aerosol type, a user can calculate a weighted mean (weighted with the squared distance to the most likely climatology mix in the domain of the three mixing fractions) or a user can select / prescribe one aerosol mix based on available measurements for a case study.

5.3 Quick start guide and user guide

This product contains in netCDF format an AVHRR Aerosol Optical Depth (AOD) dataset covering Europe and North Africa over land (10W – 50E, 35 – 60 N) for the period 01/01/2003 – 31/12/2012 inferred from 2 AVHRR/3 instruments onboard two subsequent platforms NOAA-16 and NOAA-18.

The dataset is provided on 3 processing levels: superpixels (L2B: 12 x 12 km^2 at nadir), gridded (1° x 1°) daily (L3 daily) and monthly (L3 monthly). The original lowest processing level (on selected dark field pixels) is not provided to users, but can be made available on request.

The product contains the best AOD estimate but also more detailed information on different aerosol types (most likely AOD value based on a multi-model ensemble climatology of the aerosol type and a 36 member ensemble of AOD values for a wide range of aerosol types spanning a realistic range in the atmosphere). A user can also process an application with all 36 ensemble members and then calculate the spread of the application results. Note that AOD values on the lowest processing level can be (slightly) negative reflecting radiometric calibration uncertainties and keeping un-cut AOD distributions.

The products contain on all levels sophisticated and detailed estimates of total AOD uncertainties propagated from the input L1B products and the retrieval algorithm through all levels of the processing chain. These total uncertainties can be directly used for data assimilation or to constrain a confidence interval around the AOD solutions. AOD uncertainties are also kept separated into the (relevant) different parts with different correlation structures, so that a user can conduct averaging and uncertainty propagation as suitable for the intended applications. Uncertainties include also separate values for the dominant effects (reflectance inversion, albedo estimation, aerosol type, cloud masking); also estimates of a sampling uncertainty (due to missing pixels from the cloud masking or from failed inversions) are contained.

The strongest weakness in the dataset is the significantly uncertain albedo estimation from the 3.7 micron channel which leads to significant scatter of the results (so that in the validation plots the skill of higher AOD values > 0.2 is no longer visible). However, a simple application for a 10-year time series over Europe proves the information contained in the record on larger aggregations.

Two specific elements in this dataset are the inclusion of a cloud-mask-induced uncertainty (for the first time) and the provision of a 36 member AOD ensemble for different aerosol types (similar to e.g. the MISR product).

6 Conclusions

We show here a demonstration dataset of Aerosol Optical Depth (AOD) over land over Europe and North Africa inferred from the AVHRR instrument onboard two subsequent platforms (NOAA-16, NOAA-18). The main purpose of this demonstration dataset is to illustrate the propagation of uncertainties benefitting from the methodology and the easyFCDR L1B dataset which were both developed in FIDUCEO. In terms of AOD retrieval this demonstration dataset, which can only exploit one single channel over land is as expected comparatively weak (against other more sophisticated sensors with many more observables usable for aerosol properties). However, despite very large scatter of the results we can show some skill for AOD<0.2 (where the bulk of AOD values over Europe are) and even the time series of the average for all-Europe lies within the results from other satellite records (absolute values and slight negative trend as far as such a short record allows reliable trend estimation). Further work is needed in particular to improve the estimation of directional surface albedo values as basis for the retrieval (which is done based on a statistical correlation with the surface albedo in the 3.7 µm channel which exhibits significant scatter).

Two key strengths can be demonstrated with this dataset:

(1) The FIDUCEO systematic methodology to analyse the processing chain and the propagation of uncertainties through it proved very useful to structure this analysis including the direct propagation of uncertainties from the input L1B products and as well the estimation of uncertainties from other dominant sources within the retrieval equation for which auxiliary information is used. The FIDUCEO methodology provides guidance to at least estimate (if not enough time is available to conduct comprehensive sensitivity studies) all needed properties for uncertainty propagation for the dominant effects and their correlation structures in space and time.

(2) The uncertainties in the FIDUCEO L1b AVHRR reflectances / brightness temperature easyFCDR product which contain all uncertainties grouped into 3 contributions with different correlation structures (uncorrelated “independent”, globally correlated “common” and regionally / periodically correlated “structured”) are good to manage uncertainty propagation through the different processing levels. This practical input uncertainty information is appropriate for downstream usage – the fullFCDR product contains many different detailed uncertainty contributions which would be much more demanding for a user to handle. The L1B uncertainty information provided was shown to be suitable to model during spatial / temporal aggregation the right balance between uncertainties which exhibit noise reduction and uncertainties which are pertained.

Another advantage of the demonstration dataset is that it includes an ensemble of 36 different AOD realisations of aerosol types (meant to span a realistic range of atmospheric aerosols). We provide also a weighted mean of those (as well as simple mean and the one most plausible realisation according to a multi-model based climatology of aerosol types) and use the weighted spread of AOD realisations in the ensemble to estimate the AOD uncertainty due to missing knowledge of the true aerosol type.

Finally, the demonstration dataset includes also a quantitative estimate of uncertainties induced by errors in the cloud masking after the first spatial aggregation level. For this a probabilistic cloud mask is used to calculate AOD differences with two different cloud probability thresholds for a weak and a strict cloud masking - these thresholds were experimentally optimized to allow a reasonable trade-off between sufficient coverage and (in the final output product) sufficiently strict cloud masking.

We also include a simple estimate of uncertainties due to sampling (the product of half of the difference between minimum and maximum of input AOD values and the fraction of missing pixels in a grid cell).

More work is needed to assess many details of the uncertainty propagation and to clean the different processing level products from some smaller bugs. Overall, uncertainties seem to be slightly over-estimated which may be due to slightly over-estimated input uncertainties or to missed correlations between two effects (reflectance inversion, albedo estimation), which are based on inverting the same look-up tables. In particular two of all the inputs make the largest contributions to the final uncertainties on all levels:

(1) The uncertainty of the significantly uncertain albedo estimation in the retrieval (and in particular its common part which is not reduced by averaging)
(2) The common contribution of the L1B input dataset which is by far the largest part of the total L1B uncertainty and again is not reduced by averaging; it may be possible that the relative part of this common contribution is too large.

7 References

Sogacheva, L., Popp, T., Sayer, A. M., Dubovik, O., Garay, M. J., Heckel, A., Hsu, N. C., Jethva, H., Kahn, R. A., Kolmonen, P., Kosmale, M., de Leeuw, G., Levy, R. C., Litvinov, P., Lyapustin, A., North, P., and Torres, O.: Merging regional and global AOD records from 15 available satellite products, Atmos. Chem. Phys. Discuss., https://doi.org/10.5194/acp-2019-446, in review, 2019.

Holben, B.N.; Eck, T.F.; Slutsker, I.; Tanré, D.; Buis, J.P.; Setzer, A.; Vermote, E.; Reagan, J.A.; Kaufman, Y.J.; Nakajima, T.; *et al*. AERONET—A federated instrument network and data archive for aerosol characterization. *Remote Sens. Environ.* 1998, *66*, 1–16.

Holzer-Popp, T., M. Schroedter, and G., Gesell, Retrieving aerosol optical depth and type in the boundary layer over land and ocean from simultaneous GOME spectrometer and ATSR-2 radiometer measurements, 1, Method description, Journal of Geophysical Research, 107, D21, pp. AAC16-1 – AAC16-17, 2002

Holzer-Popp T., Schroedter-Homscheidt, M., Breitkreuz, H., Klüser, L., Martynenko, D., Improvements of synergetic aerosol retrieval for ENVISAT, Atmospheric Chemistry and Physics, 8, 7651-7672, 2008

Holzer-Popp T., M. Schroedter-Homscheidt, H. Breitkreuz, D. Martynenko, and L. Klüser, Benefits and limitations of the synergistic aerosol retrieval SYNAER, in Kokhanovsky A. and de Leeuw G., Aerosol Remote Sensing over Land, Springer, Berlin, 2009

Martynenko, D., Holzer-Popp, T., Elbern, H., Schroedter-Homscheidt, M., Understanding the aerosol information content in multi-spectral reflectance measurements using a synergetic retrieval algorithm, Atmospheric Measurement Techniques, 3, 1589-1598, doi:10.5194/amt-3-1589-2010, 2010

Kriebel, K.T., Saunders, R.W. and Gesell, G., 1989: Optical properties of clouds derived from fully cloudy AVHRR pixels, *Beiträge zur Physik der Atmosphäre*, **8**, 723-729.

Kriebel K. T., Gesell G., Kästner M., and Mannstein H., 2003: The cloud analysis tool APOLLO: Improvements and Validation, *Int. J. Rem. Sens.*, **24**, 2389-2408.

Saunders, R.W., and Kriebel, K.T., 1988: An improved method for detecting clear sky and cloudy radiances from AVHRR data, *Int. Journ. Rem. Sens.*, **9**, 123-150.

Nagel, M. R., Quenzel, H., Kweta, W., Wendling, P., 1978, *Daylight Illumination-Color- Contrast-Tables*, New York, Academic Press.

Dubovik, O., Holben, B., Eck, T.F., Smirnov, A., Kaufman, Y.J., King, M.D., Tanre, D., and Slutsker, I., 2002: Variability of Absorption and Optical Properties of Key Aerosol Types Observed in Worldwide Locations, *J. Atmos. Sci.*, **59**, 590-608.

Hess, M., Köpke, P., Schult, I., 1998: Optical Properties of Aerosols and Clouds: The Software package OPAC, *Bull. Am. Met. Soc.*, **79**, 831-844

Kriebel K. T., 1977: *Reflection properties of vegetated surfaces*: Tables of measured spectral biconical reflectance factors, Wiss. Mitt., 29, Universität München.

Schnaiter, M., Horwath, H., Möhler, O., Naumann, K.-H., Saathoff, H., and Schöck, O.W., 2003: UV-VIS-NIR spectral optical properties of soot and soot-containing aerosols, *J. Aerosol Sci.*, **34**, 1421-1444.

Smith D.L. and Poulsen C.A., 2008, “Calibration Status of the AATSR Reflectance Channels”, Proceedings of MERIS/AATSR Workshop

de Leeuw, G., T. Holzer-Popp, S. Bevan, W. Davies, J. Descloitres, R.G. Grainger, J. Griesfeller, A. Heckel, S. Kinne, L. Klüser, P. Kolmonen, P. Litvinov, D. Martynenko, P.J.R. North, B. Ovigneur, N. Pascal, C. Poulsen, D. Ramon, M. Schulz, R.Siddans, L. Sogacheva, D. Tanré, G.E. Thomas, T.H. Virtanen, W. von Hoyningen Huene, M.Vountas, S. Pinnock, Evaluation of seven European aerosol optical depth retrieval algorithms for climate analysis, Remote Sensing of Environment, 2014

Holzer-Popp, T., de Leeuw, G., Martynenko, D., Klüser, L., Bevan, S., Davies, W., Ducos, F., Deuzé, J. L., Graigner, R. G., Heckel, A., von Hoyningen-Hüne, W., Kolmonen, P., Litvinov, P., North, P., Poulsen, C. A., Ramon, D., Siddans, R., Sogacheva, L., Tanre, D., Thomas, G. E., Vountas, M., Descloitres, J., Griesfeller, J., Kinne, S., Schulz, M., and Pinnock, S., Aerosol retrieval experiments in the ESA Aerosol_cci project, Atmos. Meas. Tech., 6, 1919 - 1957, doi:10.5194/amt-6-1919-2013, 2013

Thomas Popp, Gerrit de Leeuw, Christine Bingen, Christoph Brühl, Virginie Capelle, Alain Chedin, Lieven Clarisse, Oleg Dubovik, Roy Grainger, Jan Griesfeller, Andreas Heckel, Stefan Kinne, Lars Klüser, Miriam Kosmale, Pekka Kolmonen, Luca Lelli, Pavel Litvinov, Linlu Mei, Peter North, Simon Pinnock, Adam Povey, Charles Robert, Michael Schulz, Larisa Sogacheva, Kerstin Stebel, Deborah Stein Zweers, Gareth Thomas, Lieuwe Gijsbert Tilstra, Sophie Vandenbussche, Pepijn Veefkind, Marco Vountas and Yong Xue, Development, Production and Evaluation of Aerosol Climate Data Records from European Satellite Observations (Aerosol_cci), Remote Sensing, 8, 421; doi:10.3390/rs8050421, 2016